Experiments in Fluids 21 (1996) 357–362 © Springer-Verlag 1996

Optical measurement of liquid film thickness and wave velocity in liquid film flows

E. T. Hurlburt, T. A. Newell

Abstract Two optical techniques are described for measurement of a liquid film's surface. Both techniques make use of the total internal reflection which occurs at a liquid–vapor interface due to the refractive index difference between a liquid and a vapor. The first technique is used for film thickness determination. A video camera records the distance between a light source and the rays which are reflected back from the liquid–vapor interface. This distance can be shown to be linearly proportional to film thickness. The second technique measures surface wave velocities. Two photo sensors, spaced a fixed distance apart, are used to record the time varying intensity of light reflected from the liquid–vapor interface. The velocity is then deduced from the time lag between the two signals.

1 Introduction

Film flow measurements have been made using a variety of techniques including capacitance sensors (Klausner et al. 1992), conductance probes (Jayanti et al. 1990; Laurinat et al. 1984), light absorption, laser induced fluorescence (Driscoll et al. 1992), and microwaves (Roy et al. 1986). These techniques all differ in ease of use, ease of calibration, intrusiveness, accuracy, frequency response, and cost. An optical technique is outlined in this paper. The technique is non-intrusive with fast frequency response. It is easy to use, requires little calibration, and can be implemented at low cost.

The technique was used to determine the liquid film thickness and wave velocity in two-phase, annular flows. These flows are important in refrigeration, steam power, and chemical processing. Results of measurements made in an air–water flow are used to demonstrate the technique.

The method may be useful for other systems such as film coating processes where film thickness control is important. The method could be developed into a control sensor for monitoring and control of a film coating.

Received: 6 October 1995/Accepted: 15 February 1996

E. T. Hurlburt, T. A. Newell
Dept. of Mechanical and Industrial Engineering
University of Illinois at Urbana-Champaign
1206 W. Green St
Urbana, IL 61801, USA

Correspondence to: E. T. Hurlburt

The authors appreciate the support of the Air Conditioning and Refrigeration Center at the University of Illinois at Urbana-Champaign under project 45.

2 Optical principle behind the technique

The measurement technique relies on the way in which light reflectivity changes as a function of incident angle at the interface between a liquid and a vapor. When light rays pass from a medium with an index of refraction n_1 to a medium with a lower index of refraction n_2, a steep increase in reflectivity occurs for incident angles near the critical angle. Figure 1 shows this behavior for a water ($n=1.33$) to air ($n=1.00$) interface as predicted by the Fresnel relations (Brewster 1992). Both the film thickness and wave velocity measurements described below take advantage of this rapid transition to total internal reflection for precision and measurability.

3 Film thickness measurement

3.1 Measurement technique

A depiction of the film thickness measurement technique is shown in Fig. 2. A laser is aimed at a transparent white coating attached to the surface of a clear tube. This generates a point source of light, with diffuse light traveling out hemispherically toward the liquid–vapor interface. Light rays at an angle less than the critical angle are primarily transmitted, however, light rays at an angle equal to or greater than the critical angle are reflected back to the white coating.

The reflected light reaches the white coating starting at a distance R from the point source. This distance is related geometrically to the height of the liquid film and is thus used as a measure of the film thickness, h_L.

$$R = R_0 + 2h_L \tan\theta_c$$

$$\theta_c = \text{critical angle}$$

$$R_0 = 2h_{\text{Wall}} \tan\theta$$

As seen in the above relations, R depends on both the tube wall thickness and the liquid film thickness. The contribution due to the wall thickness, R_0, however, is constant and can be found by measuring R with no liquid in the tube.

To check the validity of the technique, the film thicknesses of stagnant water films were measured using the reflected light images and compared to measurements taken using calipers.

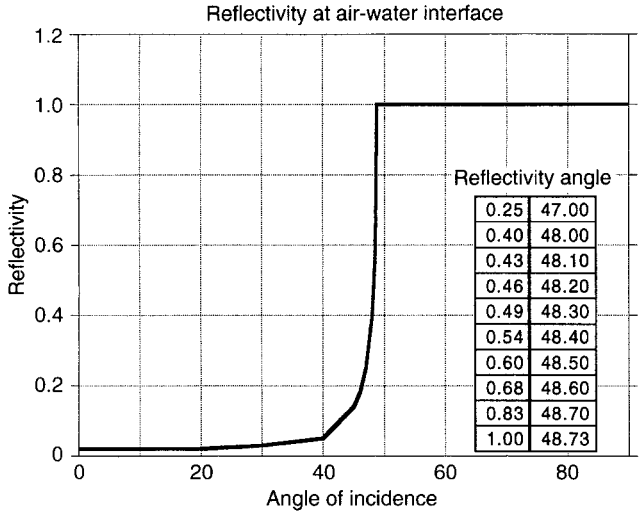

Fig. 1. Reflectivity as a function of incident angle for an air–water interface

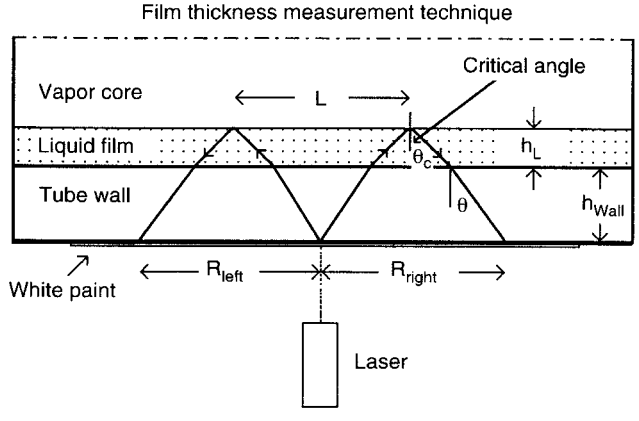

Fig. 2. Film thickness measurement technique

Over the range of measurements considered (0.5 to 1.2 cm) the two methods showed agreement to within 1%.

3.2 Film thickness data processing

Using the measurement technique described above, film thickness measurements were taken in a horizontal air–water flow loop. A schematic of the flow loop is shown in Fig. 3. Air was first drawn by vacuum through an air mass flow measurement section. After turning a U bend, water was injected into the air stream resulting in a co-current annular flow pattern. The measurement section was a clear acrylic tube with an inner diameter of 2.54 cm and a wall thickness of 0.318 cm. Measurements were taken 100 diameters downstream from the point of water injection.

A 5 mW He–Ne laser was used as the light source. The reflected light images were recorded using a standard video camera with the shutter speed set between 1/1000 and 1/10 000 of a second. For the 1/1000 of a second setting this results in 3 mm of surface translation while a frame is being captured.

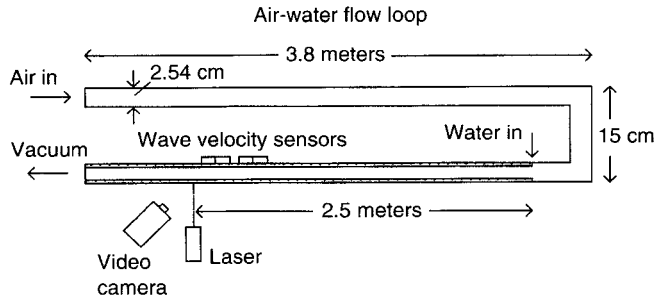

Fig. 3. Air–water flow loop

For a given operating condition, individual frames were sampled at random from the videotape by a frame grabber. This generated a bit map data file for each frame. Since a standard video camera uses interlacing, one frame actually contains two images taken 1/60 of a second apart. The two interlaced images were separated by a program into two files; one containing the odd lines and the other the even lines. These two images were then used to measure R_{left} and R_{right}, the reflected light boundary locations down the tube axis to the left and right of the point source, resulting in 4 measurements per frame.

Figure 4a shows the constant base radius location due to the tube wall thickness, R_0. The dark black object in the center is a light shield used to block light which reflects back from the point source. Figure 4b shows a typical "de-laced" image. The radius, R, is measured at the inner edge of the reflected light boundary. Note the larger radius with the liquid film present.

In some images, no high contrast boundary was observed. It is not known if this is caused by a very thick film with a very wide radius, or if this represents some other condition such as a finely rippled surface.

Approximately 16 frames were processed at each operating condition. Figure 5 shows an example of the resulting 64 realizations of the film thickness measurement. The average for this sample was 0.28 mm with a standard deviation of 0.17 mm.

Average film thicknesses measured at the bottom, side, and top of the tube for five different flow rates are shown in Table 1. Also shown is the standard deviation of the film thickness, s, and the standard error, Std Err. The standard deviation is relatively large showing the large variation in film thickness occurring in the annular flow. The standard error is an estimate of the error in the average film thickness values.

$$\text{Std Err} = 2s/\text{sqrt}(n)$$

where n = sample size.

3.3 Errors and limitations

The precision of the film thickness technique outlined above is limited by the instruments used in the measurement process and by limitations inherent to the technique.

As seen in Fig. 1, the transition to total internal reflection for an air–water interface occurs over an angle of about 1°. This causes the dark to light boundary on the measured image not to be a perfectly sharp edge. Measurement precision is limited by the resolution to which this boundary location can be

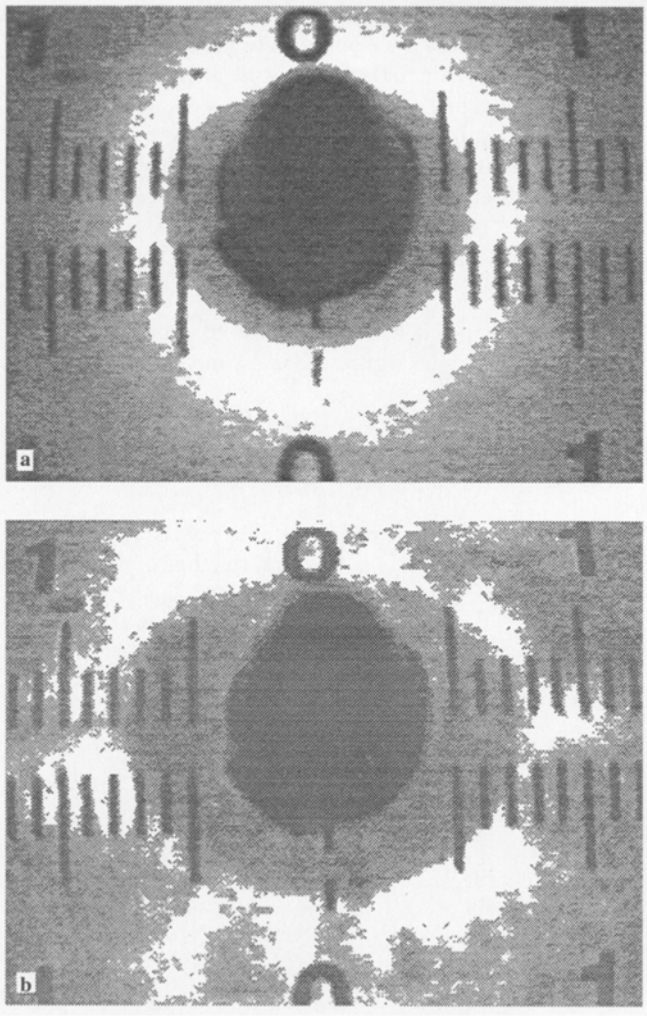

Fig. 4. **a** Calibration image with no liquid film on tube wall; **b** "De-laced" image with liquid film on tube wall

identified. For the air–water flow data presented in this paper, boundary blur resulted in an estimated 3% error in film thickness.

Another inherent limitation to the technique is the error introduced by the liquid film surface slope. The surface slope must be on the order of 5° or less in order for the error in the film thickness measurement to be less than 20%.

Film thickness measurements taken from a "de-laced" reflected image can be used to estimate the surface slope. Film thickness measurements h_{left} and h_{right} are from interface locations separated by a distance $L=(R_{\text{left}}+R_{\text{right}})/2$. If we

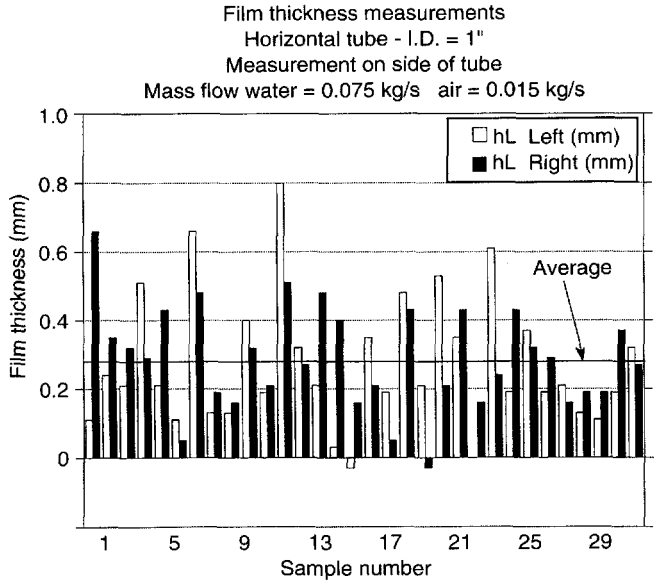

Fig. 5. Typical film thickness measurements at one operating condition

Table 1. Air–water film thickness data, horizontal pipe, I.D. = 2.54 cm

Avg film thickness (64 samples)						
$\dot{m}_{\text{water}}$ [kg/s]	$\dot{m}_{\text{air}}$ [kg/s]	h_L Bottom [mm]	h_L Side [mm]	h_L Top [mm]	h_L^* Circ Avg [mm]	Std Error [mm]
0.100	0.013	1.40	0.45	0.21	0.63	0.10
0.075	0.015	0.76	0.28	0.18	0.38	0.06
0.050	0.016	0.58	0.32	0.25	0.37	0.07
0.040	0.018	0.52	0.27	0.19	0.31	0.05
0.013	0.020	0.28	0.25	0.15	0.23	0.04
Std deviation of film thickness						
$\dot{m}_{\text{water}}$ [kg/s]	$\dot{m}_{\text{air}}$ [kg/s]	s Bottom [mm]	s Side [mm]	s Top [mm]	s^* Circ Avg [mm]	
0.100	0.013	0.68	0.23	0.18	0.39	
0.075	0.015	0.38	0.17	0.14	0.24	
0.050	0.016	0.40	0.21	0.20	0.27	
0.040	0.018	0.29	0.20	0.13	0.21	
0.013	0.020	0.20	0.13	0.15	0.16	

*Side values used twice when calculating average around circumference

assume this spacing is small relative to the wavelength, the surface slope can be estimated by $(h_{left}-h_{right})/L$. For the air–water flow data of Fig. 5 the maximum slope is 5° and the average is about 1.5°.

Other sources of error are the uncertainty in the value of the index of refraction of the liquid and the vapor, processed image resolution, and the motion of the liquid film while the shutter is open. These errors are not inherent to the technique and can be reduced if necessary to achieve higher precision.

4
Wave velocity measurement

4.1
Measurement technique

Figure 6 shows the sensor arrangement used to measure wave velocity. Two high brightness light emitting diodes (1500 mcd, 680 nm) spaced axially a fixed distance apart are attached to the tube. Two 3 mm × 3 mm Hamamatsu Photonics S1133 photo cells are also attached to the tube with their surfaces covering the regions in which the LED's light will be reflected from the liquid–vapor interface. Since the voltage output from the photo cell depends on the total light incident on the cell's surface, the cell output voltage depends on the film thickness and wave structure.

As a wave propagates downstream it passes over each of the photo cells. If the cell spacing is sufficiently small, the wave characteristic changes very little over the distance between the two cells. Thus, waves induce nearly identical voltage outputs in each of the photo cells. Using statistical methods, the time lag at which the signals are nearly identical can be determined. This time lag along with the known spacing of the photo cells is then used to calculate the velocity of the waves on the liquid surface.

4.2
Data processing

Wave velocity measurements were taken in the horizontal air–water flow loop described in Sect. 3.2. As with film thickness, the measurements were taken 100 diameters downstream from the point of water injection.

An example of the signal from one photo cell is shown in Fig. 7. The voltage is not constant due to variations in film thickness and surface angle which affect the amount of reflected light incident on the photo cell. Also, since the length of the photo cell is of the same order as the movement of the reflected light boundary, the output is not linearly proportional to film thickness. This makes it difficult to interpret the meaning of the signal's magnitude.

Figure 8 shows the overlaid output from both photo cells. The time lag between signals x and y is found by calculating a correlation coefficient based on the cross correlation function.

$$R_{xy}(\tau)=E[(x(t)-\mu_x)(y(t+\tau)-\mu_y)]$$

Here, t is time and τ is the shift in time of signal y.

When using a digital signal, R_{xy} is estimated by the cross correlation estimator.

$$R_{xy}(\tau)=1/(N-r)\sum_{n=1}^{N-r}[(x_n-\mu_x)(y_{n+r}-\mu_y)]$$

In this equation, r is the number of data points by which y is shifted back in time and N is the total number of data points.

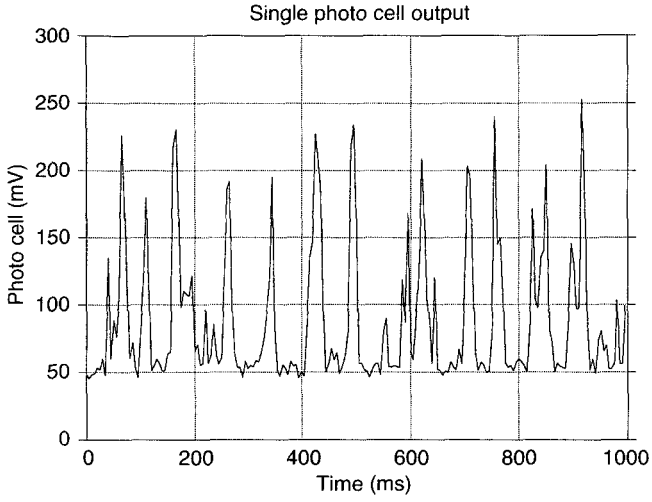

Fig. 7. Signal from one photo cell

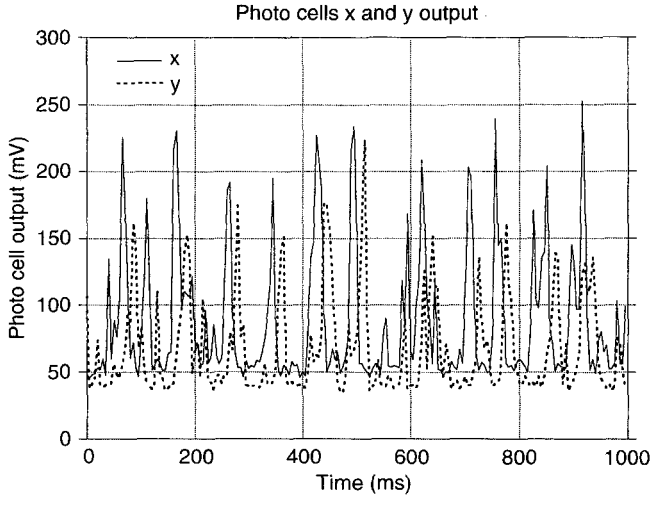

Fig. 8. Overlaid signals from two photo cells spaced 5 cm apart

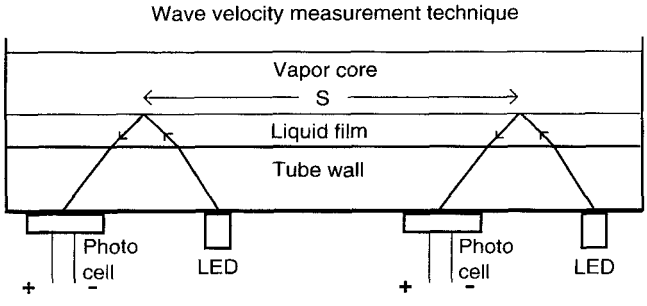

Fig. 6. Wave velocity measurement diagram

Dividing by the standard deviation of the signals gives the correlation coefficient, ρ_{xy}.

$$\rho_{xy}(\tau) = R_{xy}(\tau)/(\sigma_x \sigma_y)$$

Figure 9 shows the correlation coefficient for the signals shown in Fig. 8. The time at which this function reaches a maximum, τ_{max}, is the time lag between signals x and y. Using τ_{max}, the wave velocity is calculated (Bendat and Pearsol 1986).

$$V_w = S/\tau_{max}$$

where S = the distance between measurement locations. From Fig. 9 we see that the time at which the correlation coefficient is a maximum is 20 ms, indicating a wave velocity of 2.50 m/s.

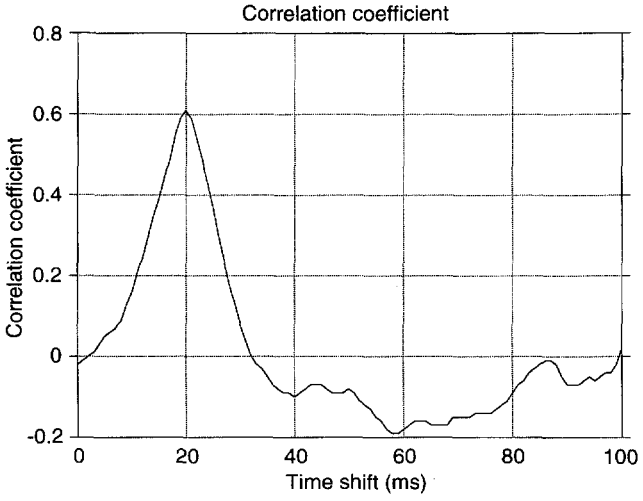

Fig. 9. Correlation coefficient function

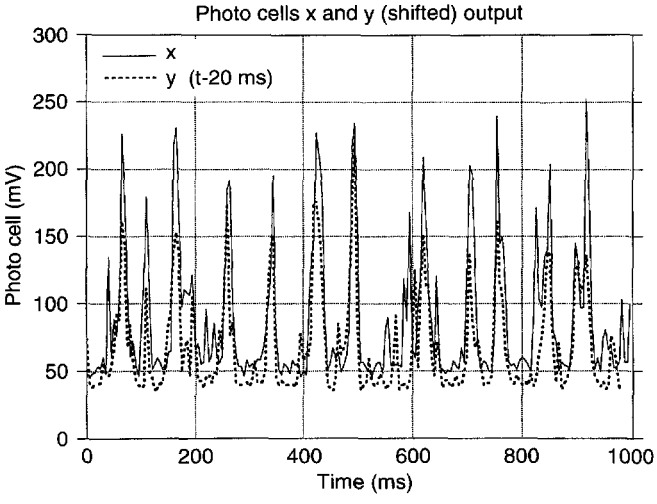

Fig. 10. Overlaid signals from two photo cells with time shift of signal y

Figure 10 shows signal x and signal y with signal y shifted by τ_{max}. The signals are similar but not identical, so they do not overlay precisely.

Wave velocities measured at the bottom, side, and top of the tube for five different flow rates are shown in Table 2. Each wave velocity was calculated by ensemble averaging 40 correlation coefficient functions, each spanning a 125 ms window, and then finding the time at which the averaged function reaches its maximum.

4.3 Limitations

The wave velocity measurement relies on the fact that waves maintain a degree of coherence as they travel downstream. A strong correlation can only be found if the wave structure passing the first photo cell does not evolve into an entirely different wave structure by the time it reaches the second photo cell.

For the air–water annular flow data shown above, the waves showed sufficient coherence over the 5 cm distance between the photo cells for a strong correlation to occur. This may not be the case for all liquid–vapor pairs or all flow regimes.

The finite width of the correlation coefficient function shown in Fig. 9 indicates that some change in wave structure occurs as the wave moves from the first to the second photo cell. This change could be the result of the growth or decay of the waves due to forces acting on the liquid. The finite width may also be the result of waves with different velocities passing down the tube. Jayanti explored this by calculating the correlation coefficient as a function of frequency instead of time (Jayanti et al. 1990). The time based correlation coefficient used in this study is limited to an estimate of the average wave velocity.

5 Conclusion

The optical technique outlined above can be used to measure film thickness and wave velocity of liquid flows. It is a relatively simple, non-intrusive method. The film thickness technique is

Table 2. Air–water wave velocity data, horizontal pipe, I.D. = 2.54 cm

Ensemble average – 40 sets – each 125 ms in width					
$\dot{m}_{water}$ [kg/s]	$\dot{m}_{air}$ [kg/s]	V_w Bottom [m/s]	V_w Side [m/s]	V_w Top [m/s]	V_w^* Circ Avg [m/s]
0.100	0.013	3.0	3.2	3.2	3.2
0.075	0.015	2.8	2.9	3.1	2.9
0.050	0.016	2.6	2.9	2.8	2.8
0.040	0.018	2.6	2.8	2.8	2.8
0.013	0.020	2.5	2.5	N/A	2.5

*Side values used twice when calculating average around circumference

limited to flows with surface slopes less than about 5°. The wave velocity technique is limited to flows which exhibit wave structure coherence over a distance of several centimeters.

Application of the technique is not limited to the two-phase flow application for which it was developed. It can be used on any transparent film flow or transparent coating system which has an overlying medium with a lower index of refraction.

References

Bendat JS; Pearsol AG (1986) Random Data: Analysis and Measurement Procedures, 2nd Edition (Revised and Expanded). Wiley, New York

Brewster MQ (1992) Thermal Radiative Transfer and Properties. Wiley, New York

Driscoll DI; Schmitt RL; Stevenson WH (1992) Thin flowing liquid film thickness measurement by laser induced fluorescence. J of Fluids Engr 114: 107–112

Jayanti S; Hewitt GF; White SP (1990) Time-dependent behaviour of the liquid film in horizontal annular flow. Int J Multiphase Flow 16: 1097–1116

Klausner JF; Zeng LZ; Bernhard DM (1992) Development of a film thickness probe using capacitance for asymmetrical two-phase flow with heat addition. Rev Sci Instrum 63: 3147–3152

Laurinat JE; Hanratty TJ; Dallman JC (1984) Pressure drop and film height measurements for annular gas–liquid flow. Int J Multiphase Flow 10: 341–356

Roy RP; Ku J; Kaufman I; Shukla J (1986) Microwave method for measurement of liquid film thickness in gas–liquid flow. Rev Sci Instrum 57: 952–956